technology · applications · instrumentation

corporation

ANALYSIS AND DESIGN OPTIMIZATION

OF THE 1.2m X-RAY TELESCOPE

FINAL REPORT, VOL. I

By

Dietrich Korsch
TAI CORPORATION
8302 Whitesburg Dr.
Huntsville, Al. 35802

Prepared For

NATIONAL AERONAUTICS AND SPACE ADMINISTRATION
MARSHALL SPACE FLIGHT CENTER, ALABAMA

Contract NA8-32829

July 1978

(NASA-CR-150775) ANALYSIS AND DESIGN OPTIMIZATION OF THE 1.2m X-RAY TELESCOPE, VOLUME 1 Final Report (TAI Corp., Huntsville, Ala.) 42 p HC A03/MF A01 CSCL 03A G3/89

N78-31020

Unclas 29175

SUMMARY

This volume summarizes the results of an image space analysis and optimization and of a performance analysis of the telescope assembly in the presence of various alignment errors. It also includes a brief study on possible test arrangments for 1.2m or 1.5m diameter x-ray telescopes. Omitted is a summary of the work that was done on the test flats because of its tentative state and because much of it was already out of date at the time this report was prepared.

TABLE OF CONTENTS

LIST OF FIGURES

LIST OF TABLES

1. INITIAL TELESCOPE ANALYSIS

Design parameters for all six subsystems compatible with the input requirements of the ray trace program KROGRAZ were generated from data provided by SAO to MFSC. The most important parameters together with some analytical results are summarized in Table 1.1. Fig. 1.1 illustrates the geometric meaning of the following parameters:

ρ_{01}: Center radius of primary,

ρ_{02}: Center radius of secondary,

d : Center to center distance,

b : Back focal distance

γ : Grazing angle at the center of each element.

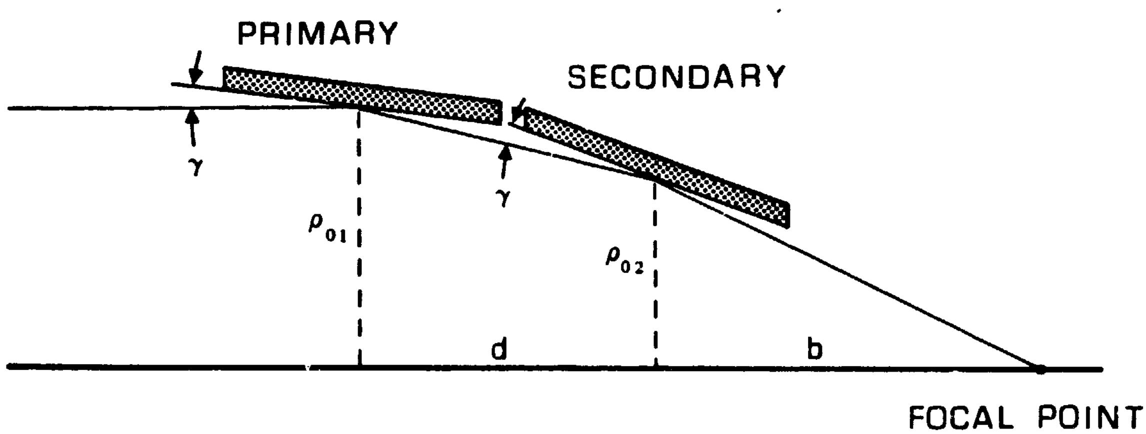

Fig. 1.1: Two-Mirror Grazing Incidence System with Design Parameters

A ray trace analysis was performed to first find the best focal surface of all individual subsystems and then determine the optimum positions of image planes such that the rms spot size on axis does not exceed 0.5 arcsec. The corresponding distances of these image planes from the gaussian focal point and the maximum achievable half field angles providing a spot size of no more than 0.5 arcsec for every individual subsystem are included in Table 1. An illustration of the image space geometry is shown in Fig. 1.2. For these analyses a reflectivity of 1 was assumed for all surfaces.

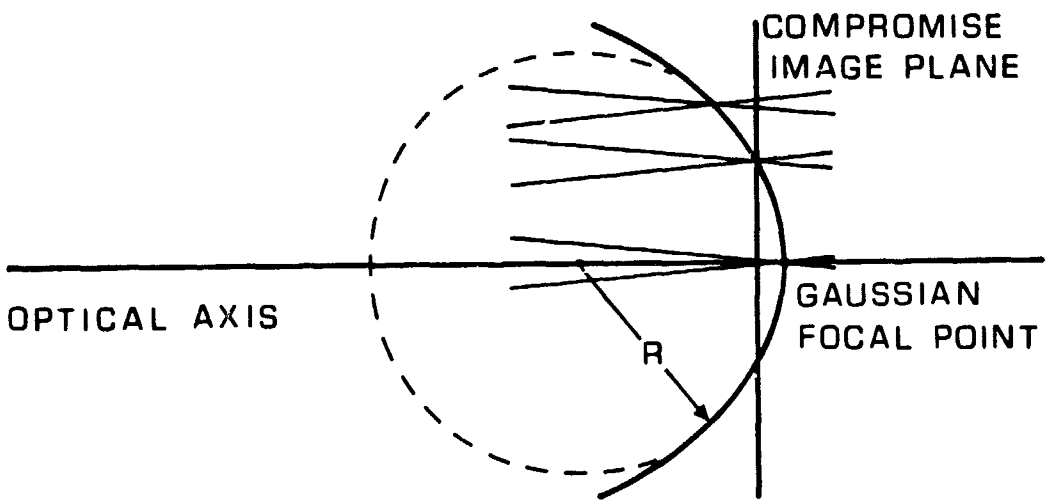

Fig. 1.2: Meridional Section of Image Surface
(R = Radius of Image Curvature)

TABLE 1.1: System Parameters

SUBSYSTEM			1	2	3	4	5	6
Center Radius of First Mirror		(in.)	23.88	21.53	19.23	16.93	14.78	12.63
Center Radius of Second Mirror		(in.)	22.8273	20.5671	18.3590	16.2026	14.0971	12.0420
Center to Center Distance		(in.)	35.0762	35.6091	36.0765	36.4822	36.8296	37.1223
Back Focal Distance		(in.)	380	380	380	380	380	380
Graz. Angle at Center of each El.		(mrad)	15.0000	13.5178	12.0689	10.6531	9.2702	7.9197
Half Width of Entrance Annulus		(in.)	0.24	0.22	0.20	0.175	0.15	0.125
Image Curvature		$(in.^{-1})$	-0.262	-0.328	-0.417	-0.538	-0.730	-0.018
Focal Length		(in.)	398.957	398.957	398.957	398.957	398.957	398.957
Collecting Area		$(in.^{2})$	71.98	59.49	48.30	37.32	27.85	19.83
Optimized for .5 arcsec in Flat Field	Dist. of Im. Pl. Gaussian Focal P.	$(10^{-3}in.)$	-8.0	-8.9	-9.9	-11.3	-12.9	-15.1
	Max. Half Field Angle	(arcmin)	2.5	2.4	2.25	2.10	2.00	1.85

Image field curvature is known to be the predominant aberration in grazing incidence telescopes. To illustrate the dependence of the curvature on the diameter of the system, the meridional sections of the image surfaces of the individual systems are shown in Fig. 1.3 in actual size.

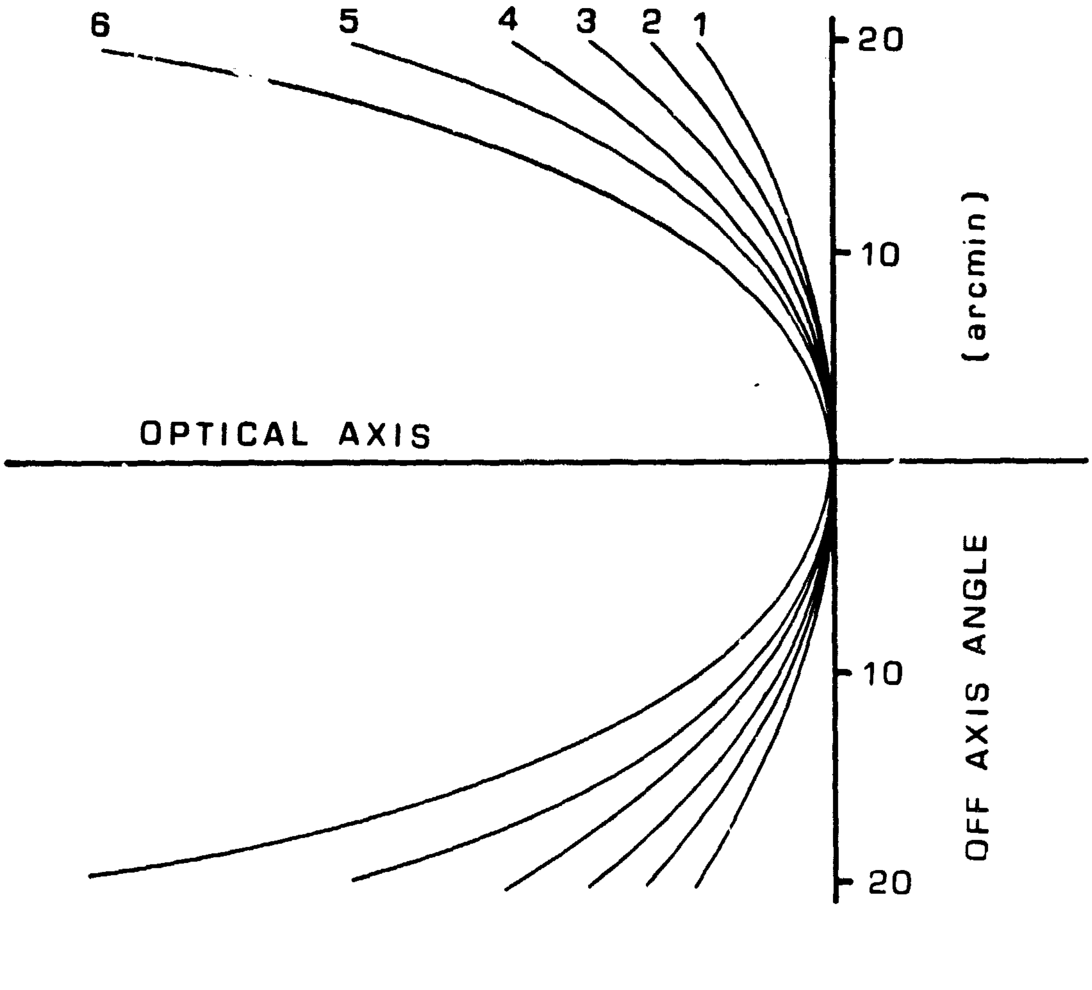

Fig. 1.3: Meridional Sections of the Image Surfaces of all Individual Subsystems (Actual Size)

The field extends over about $\pm$ 20 arcmin. The resultant optimum focal surface of the compound system is shown in Fig. 1.4. It is also drawn in actual size and includes the rms-spot sizes at different field positions up to 20 arcmin. Fig. 1.4 was generated by letting each subsystem contribute according to its geometric collecting area. The result is expected to change, however, when the effective collecting areas which depend strongly on the grazing angle and the surface material are taken into account.

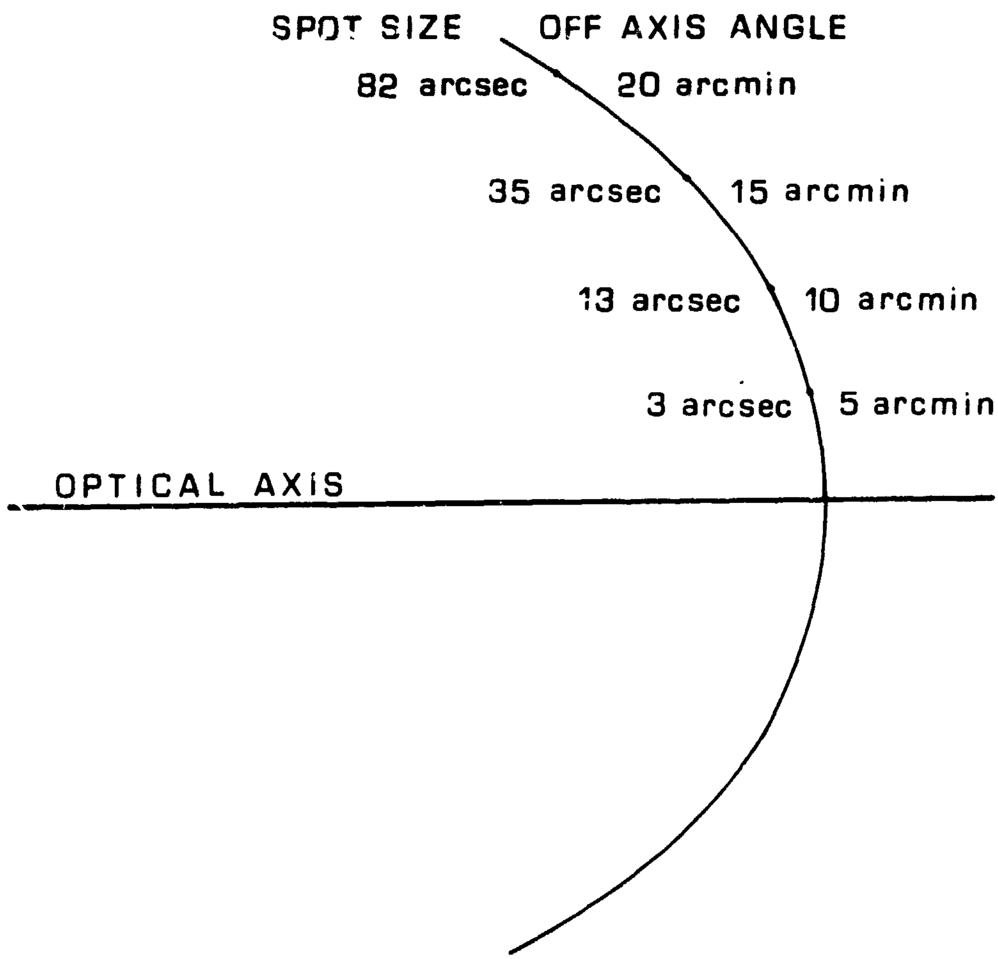

Fig. 1.4: Meridional Section of the Optimum Focal Surface Formed by all Six Subsystems

2. REFLECTIVITY AND EFFECTIVE AREA

The reflectivities and effective areas (geometric area x reflectivity) of the six telescope subsystems were determined for two coating materials and four wavelengths. The reflectivities, R, were calculated according to*,

$$R = R_1\ (1+R_0)/2,$$

with

$$R_1 = (4a^2(s-a)^2 + V)/\ (4a^2(s+a)^2 + V),$$

$$R_0 = (4a^2(t-a)^2 + V)/\ (4a^2(t+a)^2 + V),$$

$$a^2 = (s^2-U+\ \ (s^2-U)^2 + V)/2,$$

$$s = \sin\gamma$$

$t = \cos\gamma/\tan\gamma$, γ being the grazing angle.

The following U - and V - values were provided by L. VanSpeybroeck, SAO:

	Au		Ni	
Å	U	V	U	V
2	1.54687E-4	6.21530E-10	8.41236E-5	8.12310E-12
10.44	2.57412E-3	1.13329E-6	1.73944E-3	7.7305E-7
47.68	2.39684E-2	4.38718E-4	2.95621E-2	2.27016E-4
103.32	1.3276E-1	1.09378E-3	7.16910E-2	1.08618E-2

The computed reflectivities and effective areas are summarized on the next two pages.

*B.L. Henke, Phys, Review A, 6, .94(1972)

AU

ORIGINAL PAGE IS
OF POOR QUALITY

WAVELENGTH (A): 2

SYSTEM	GRAZ ANG (RAD)	REFLECTIVITY	EFF AREA (SQ IN)
1	0.015	0.079709582	5.737481332
2	0.013517768	0.174547064	10.38380484
3	0.012068919	0.413908125	19.99176245
4	0.010653141	0.605363702	22.59217336
5	9.27015E-03	0.705747147	19.65505804
6	7.91969E-03	0.771243543	15.29375947

TOTAL EFF AREA : 93.65403948

WAVELENGTH (A): 10.44

SYSTEM	GRAZ ANG (RAD)	REFLECTIVITY	EFF AREA (SQ IN)
1	0.015	0.793923223	57.14659356
2	0.013517768	0.813529435	48.39686606
3	0.012068919	0.832741237	40.22140172
4	0.010653141	0.851597144	31.7816054
5	9.27015E-03	0.870130579	24.23313663
6	7.91969E-03	0.888370439	17.6163858

TOTAL EFF AREA : 219.3959892

WAVELENGTH (A): 47.68

SYSTEM	GRAZ ANG (RAD)	REFLECTIVITY	EFF AREA (SQ IN)
1	0.015	0.886549686	63.81384640
2	0.013517768	0.897215487	53.37534932
3	0.012068919	0.907748657	43.84426014
4	0.010653141	0.918146716	34.26523543
5	9.27015E-03	0.928406950	25.85613356
6	7.91969E-03	0.938526412	18.61097875

TOTAL EFF AREA : 239.7658036

WAVELENGTH (A): 103.32

SYSTEM	GRAZ ANG (RAD)	REFLECTIVITY	EFF AREA (SQ IN)
1	0.015	0.980027911	70.54240905
2	0.013517768	0.981986039	58.41834947
3	0.012068919	0.983903093	47.52251941
4	0.010653141	0.985779363	36.78928582
5	9.27015E-03	0.987615096	27.50508042
6	7.91969E-03	0.989410501	19.62001023

TOTAL EFF AREA : 260.3976544

NI

WAVELENGTH (A): 2

SYSTEM	GRAZ ANG (RAD)	REFLECTIVITY	EFF AREA (SQ IN)
1	0.015	0.013589083	0.978142211
2	0.013517768	0.023429777	1.393837450
3	0.012068919	0.045028034	2.174854045
4	0.010653141	0.105957417	3.954330797
5	9.27015E-03	0.498928581	13.89516098
6	7.91969E-03	0.890820653	17.66497354

TOTAL EFF AREA : 40.06129902

WAVELENGTH (A): 10.44

SYSTEM	GRAZ ANG (RAD)	REFLECTIVITY	EFF AREA (SQ IN)
1	0.015	0.716278549	51.55772994
2	0.013517768	0.742726777	44.18481595
3	0.012068919	0.768706453	37.12852167
4	0.010653141	0.794281523	29.64258643
5	9.27015E-03	0.819508196	22.82330326
6	7.91969E-03	0.844435784	16.7451616

TOTAL EFF AREA : 202.0821188

WAVELENGTH (A): 47.68

SYSTEM	GRAZ ANG (RAD)	REFLECTIVITY	EFF AREA (SQ IN)
1	0.015	0.924563678	66.55009354
2	0.013517768	0.931795926	55.43253965
3	0.012068919	0.938908164	45.3492643
4	0.010653141	0.945900388	35.30100249
5	9.27015E-03	0.952772399	26.5347113
6	7.91969E-03	0.959523798	19.0273569

TOTAL EFF AREA : 248.1949682

WAVELENGTH (A): 103.32

SYSTEM	GRAZ ANG (RAD)	REFLECTIVITY	EFF AREA (SQ IN)
1	0.015	0.919869111	66.21217858
2	0.013517768	0.927499766	55.17696107
3	0.012068919	0.935017471	45.16134384
4	0.010653141	0.942420515	35.1711336
5	9.27015E-03	0.949707097	26.44934266
6	7.91969E-03	0.956875325	18.9748377

TOTAL EFF AREA : 247.1457974

ORIGINAL PAGE IS
OF POOR QUALITY

3. FOCAL PLANE OPTIMIZATION

The analyses described in this chapter were performed by tracing rays through all six subsystems simultaneously whereby the number of rays for each subsystem was proportional to its effective area.

Since each individual subsystem of the telescope assembly has a different focal surface with the field radii increasing with increasing aperture diameters, the field radius of the nested system will fall somewhere between the radii of the outer and inner systems, depending on the contributions of each of the six subsystems to the total effective area. Because the subsystem contributions to the collecting area are functions of their reflectivities, and thus functions of the wavelength, the field radius of the optimum system focal surface is expected to be wavelength dependent. The best-focus performances and field radii of the nested system for two surface materials (Au and Ni) and four different wavelengths are represented by the curves numbered 1 in Figures 3.2 to 3.8.

To find the optimum position of an assumed flat detector surface, two analytical approaches were pursued.

a) The Common Focal Point Configuration

The system is aligned so that all six subsystem focal points coincide (See Figure 3.1a). The detector surface is moved toward the telescope until the on-axis rms-spot diameter reaches 0.5 arcsec.

The flat-field performances for this focal plane configuration are represented by the number 2 curves in Fig. 3.2 to 3.8. The respective detector shift, Δ b, from the common focal point is also given on the diagram.

b) The Staggered Focal Point Configuration

The image plane positions for an on-axis rms-spot size of 0.5 arcsec are determined for each subsystem separately. Matching the six image planes then resulted in a staggered focal point array (see Fig. 3.1 b). The individual image plane shifts from the respective focal points are then constant and wavelength independent. These respective shifts are from the outer to the inner subsystem:

$$\Delta b_1 = -0.0080 \text{ in.},$$
$$\Delta b_2 = -0.0089 \text{ in.},$$
$$\Delta b_3 = -0.0099 \text{ in.},$$
$$\Delta b_4 = -0.0113 \text{ in.},$$
$$\Delta b_5 = -0.0129 \text{ in.},$$
$$\Delta b_6 = -0.0151 \text{ in.}.$$

The number 3 curves in Figures 3.2 to 3.8 show the flat-field performance of the staggered focal point configuration for the two metals and the four wavelengths.

Even though the difference between the common focal point configuration and the staggered focal point configuration seems to be insignificant, the wavelength independence of the second configuration must be regarded a definite advantage since it avoids the focus change that is required for different wavelengths when using the first configuration.

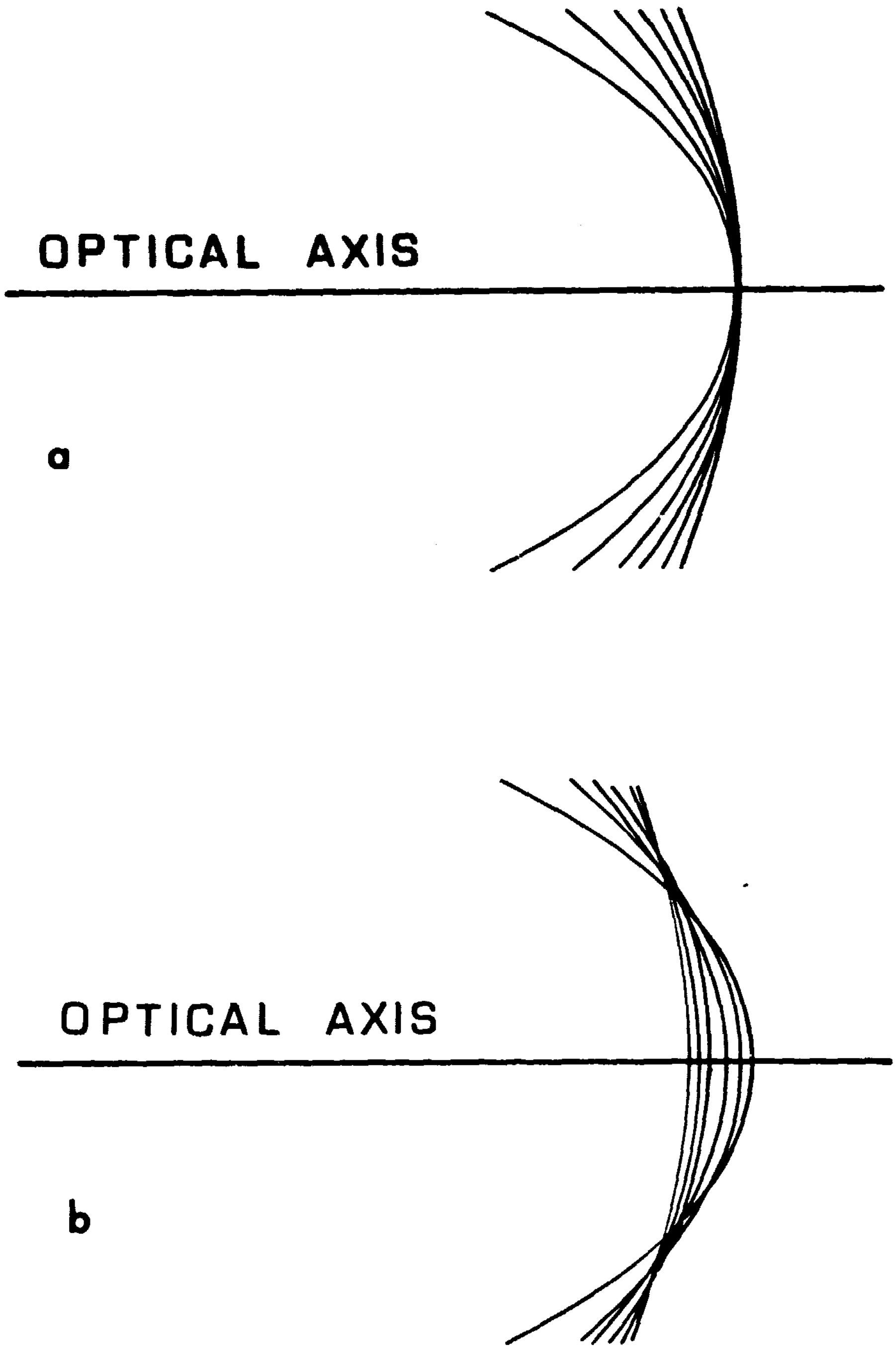

Fig. 3.1: Two Focal Surface Configurations:
a) Common Foci
b) Staggered Foci

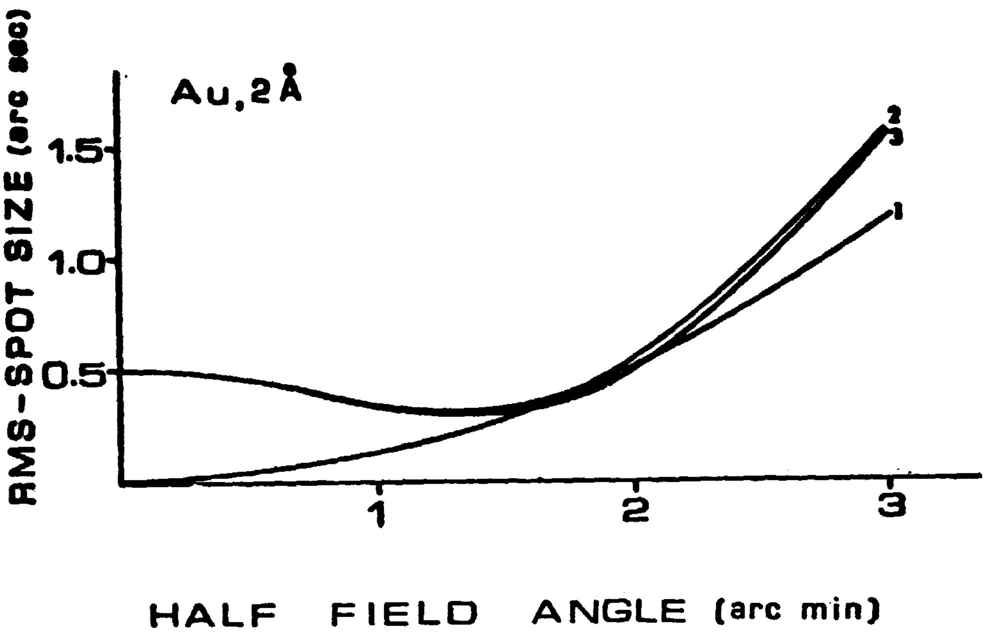

Fig. 3.2: Off-Axis Performance: (1) Best Focus (Field Radius = -1.65 in.), (2) Flat Field, Common Foci (Focal Shift = -0.012 in.), (3) Flat Field, Staggered Foci.

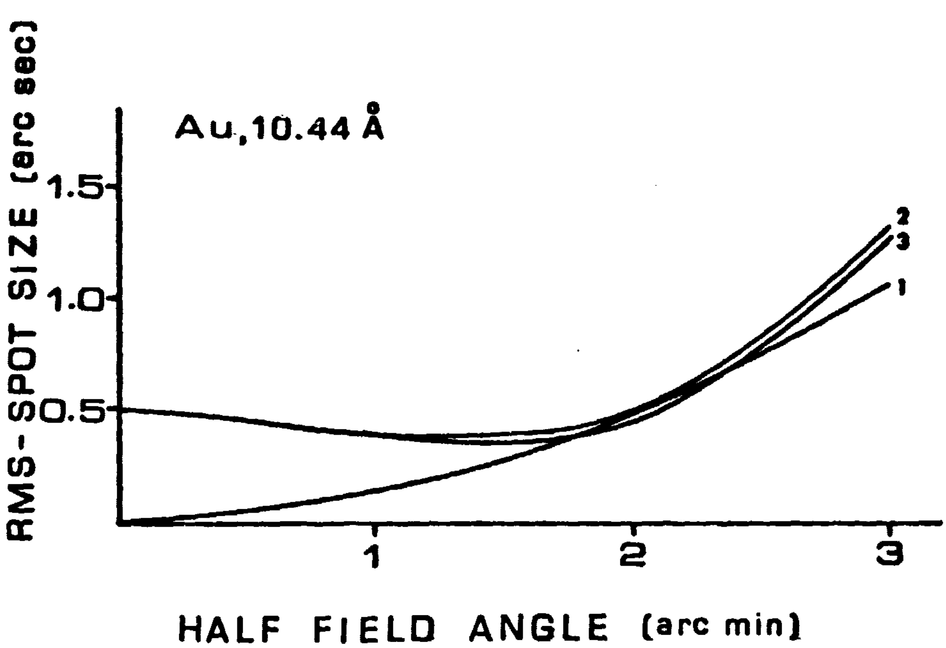

Fig. 3.3: Off-Axis Performance: (1) Best Focus (Field Radius = -2.41 in.), (2) Flat Field, Common Foci (Focal Shift = -0.010 in.), (3) Flat Field, Staggered Foci.

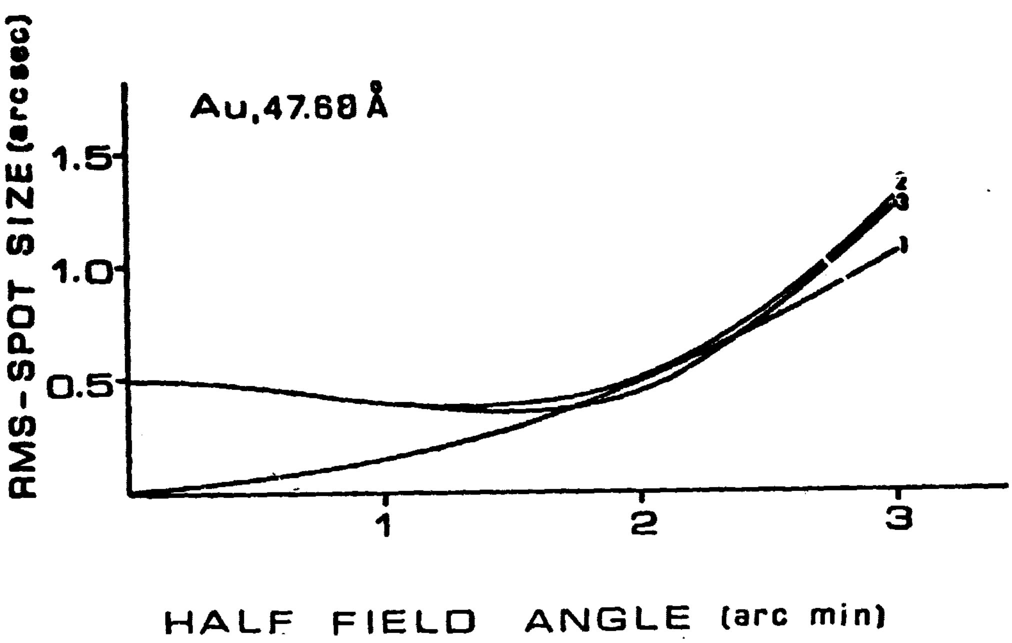

Fig. 3.4: Off-Axis Performance: (1) Best Focus (Field Radius = -2.44 in.), (2) Flat Field, Common Foci (Focal Shift = -0.010 in.), (3) Flat Field, Staggered Foci.

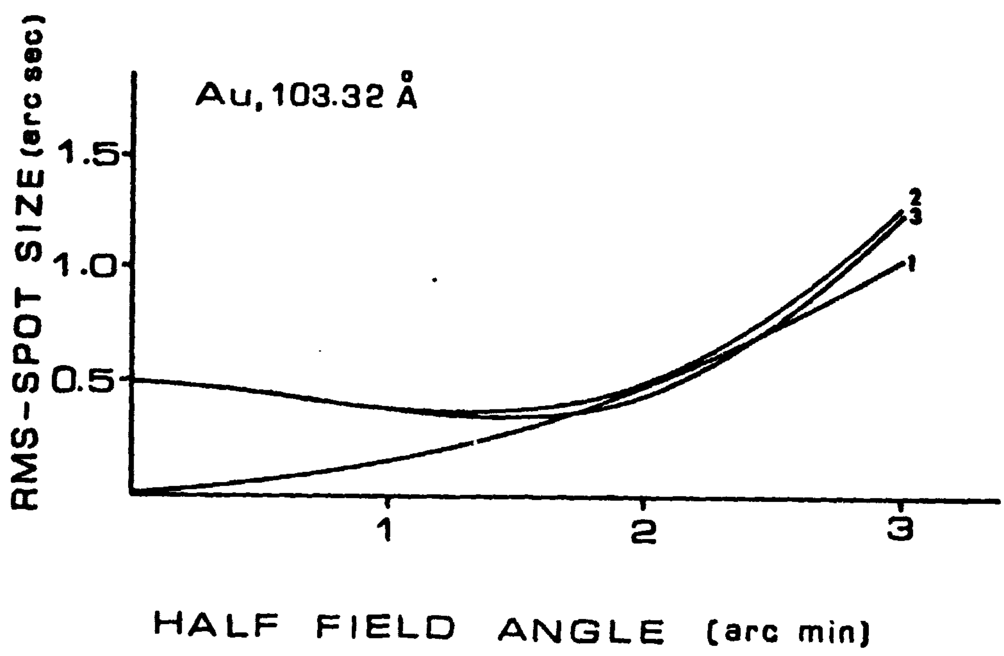

Fig. 3.5: Off-Axis Performance: (1) Best Focus (Field Radius = -2.44 in.), (2) Flat Field, Common Foci (Focal Shift = -0.010 in.), (3) Flat Field, Staggered Foci.

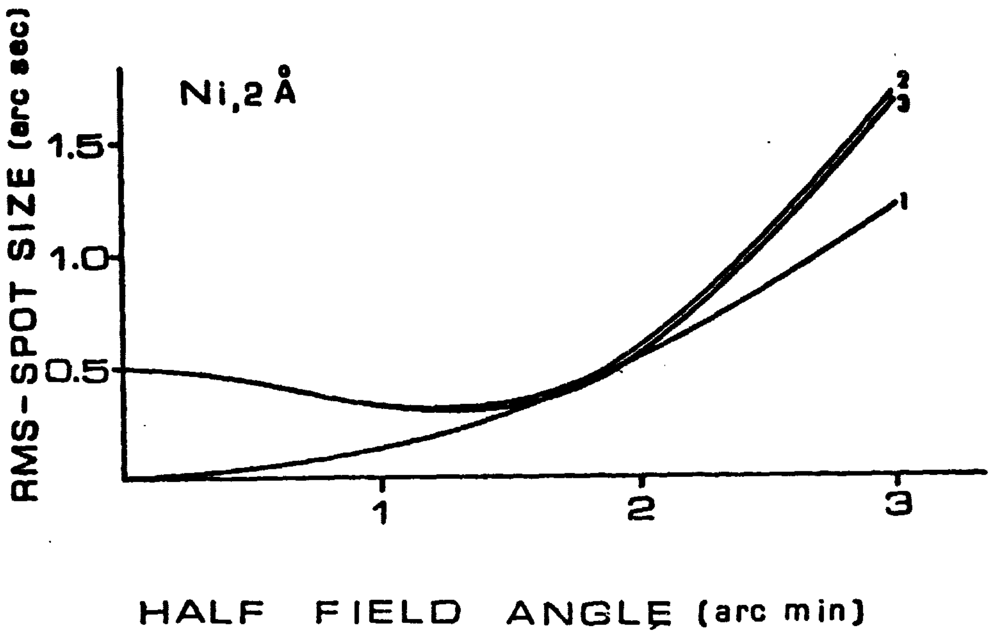

Fig. 3.6: Off-Axis Performance: (1) Best Focus (Field Radius = -1.35 in.), (2) Flat Field, Common Foci (Focal Shift = -0.013 in.), (3) Flat Field, Staggered Foci.

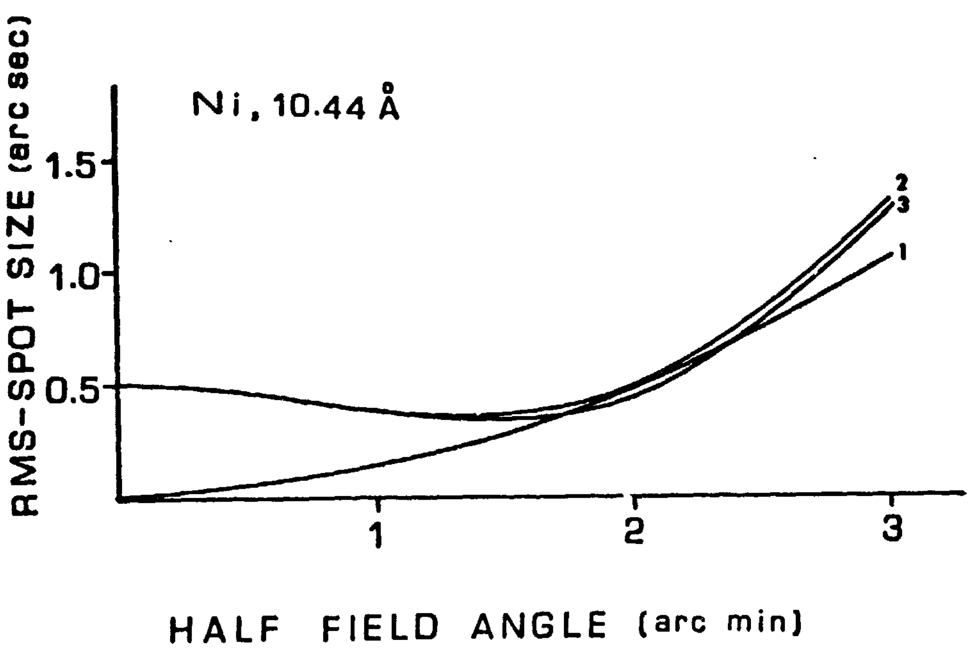

Fig. 3.7: Off-Axis Performance: (1) Best Focus (Field Radius = -2.38 in.), (2) Flat Field, Common Foci (Focal Shift = -0.010 in.), (3) Flat Field, Staggered Foci.

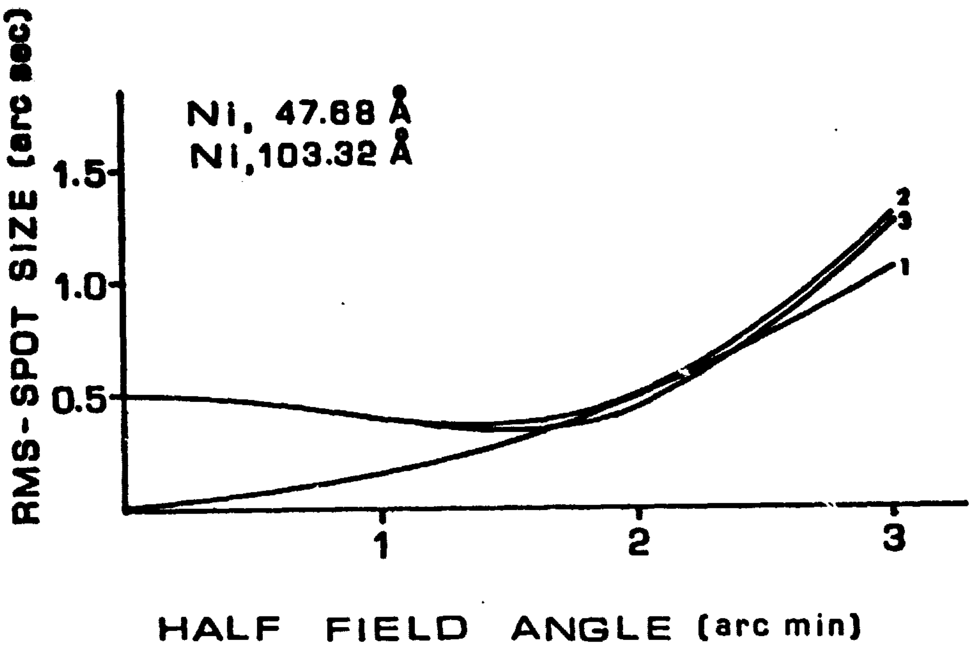

Fig. 3.8: Off-Axis Performance: (1) Best Focus (Field Radius = -2.43 in.), (2) Flat Field, Common Foci (Focal Shift = -0.010 in.), (3) Flat Field, Staggered Foci.

4. EFFECTS OF MISALIGNMENTS ON THE PERFORMANCE

The effects of misalignments on the telescope performance were investigated in two ways. First the misalignment sensivities, i.e., the effects of linear and angular alignment errors between primary and secondary on the focal plane performance of the individual subsystems were established. Then the performance of the entire nested array was determined while each of the twelve mirror elements was randomly misaligned within certain preset limits.

4.1 ALIGNMENT SENSITIVITIES

The following table summarizes the increases of the spot size due to various isolated misalignments between the primary and secondary mirrors of all subsystems.

TABLE 4.1: Misalignment Sensitivities

		DESPACE	DECENTER	TILT
RMS SPOT SIZE INCREASE	SYSTEM 1	0.015 μrad/μm	0.1 μrad/μm	1.9 μrad/μrad
	SYSTEM 2	0.013 μrad/μm	0.1 μrad/μm	1.9 μrad/μrad
	SYSTEM 3	0.012 μrad/μm	0.1 μrad/μm	1.9 μrad/μrad
	SYSTEM 4	0.010 μrad/μm	0.1 μrad/μm	1.9 μrad/μrad
	SYSTEM 5	0.09 μrad/μm	0.1 μrad/μm	1.9 μrad/μrad
	SYSTEM 6	0.08 μrad/μm	0.1 μrad/μm	1.9 μrad/μrad

All spot sizes were established in a fixed gaussian focal plane.

4.2 RANDOM ALIGNMENT ERRORS

The purpose of this experiment is to predict the most probable performance of a real system where each component can only be aligned to within certain limits with regard to the perfect design. In the computer simulation each of the twelve mirror elements was therefore allowed to be out of alignment with respect to five degrees of freedom and within given limits. The five degrees of freedom were shared by two tilts about the center of each element in the x, z - and y, z planes, and linear shifts along the three axes. The random misalignment values were generated by multiplying a given limit value for every degree of freedom with a computer generated random number between -1 and +1. One hundred computer runs per set of limit values, each determining the rms spot size of the entire telescope system were then made. The performance predictions for various misalignments are shown in Figs. 4.1 to 4.7. While some runs were made where the computer automatically searched for the plane of best focus, other analyses were done in a fixed gaussian focal plane. The first four graphs show the performance for angular misalignments of 5 μrad (1 arcsec) and linear misalignments (decenter and despace) of 0.001 in. In the following two runs the tilt and decenter limit values were varied successively to appreciate there individual contributions. The final plot shows a set of misalignment limits that yield a spot size in the order of 1 arcsec.

ORIGINAL PAGE IS
OF POOR QUALITY

Fig. 4.1: Probable Performance for the Following Limit Values:
Tilt = 5 μrad
Decenter = 0.001 in.
Despace = 0.001 in.
(On Axis, Best Focus)

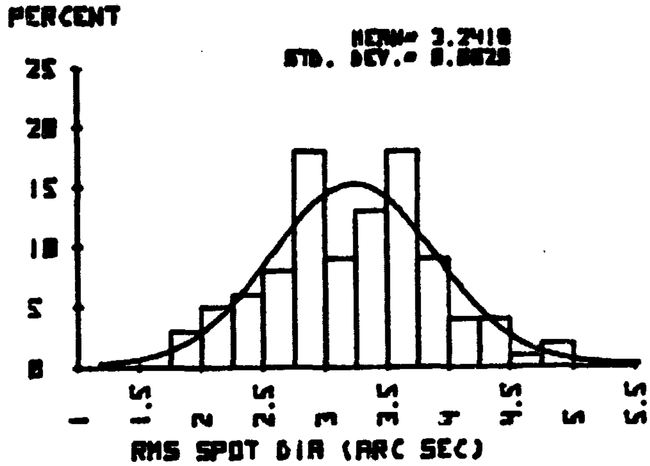

Fig. 4.2: Probable Performance for the Following Limit Values:
Tilt = 5 μrad
Decenter = 0.001 in.
Despace = 0.001 in.
(On Axis, Fixed Focus)

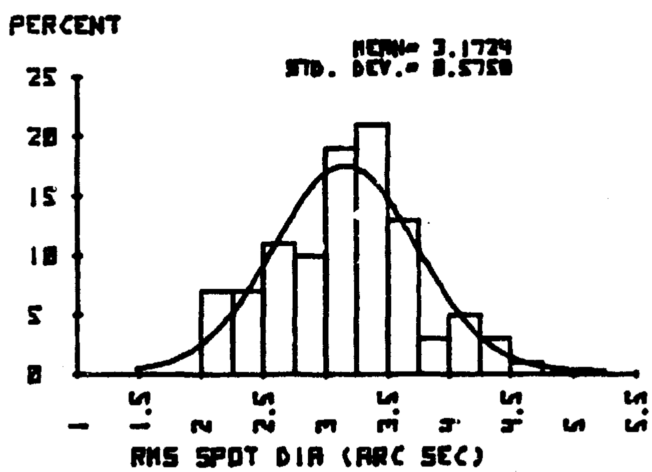

Fig. 4.3: Probable Performance for the Following Limit Values:
Tilt = 5 μrad
Decenter = 0.001 in.
Despace = 0.001 in.
(2 arcmin Off Axis, Best Focus)

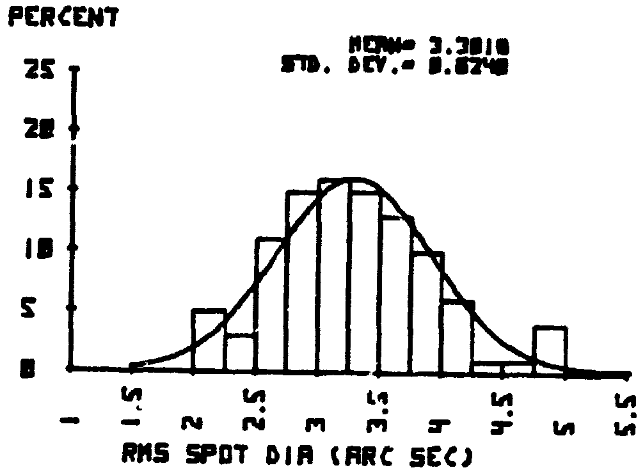

Fig. 4.4: Probable Performance for the Following Limit Values:
Tilt = 5 μrad
Decenter = 0.001 in.
Despace = 0.001 in.
(2 arcmin Off Axis, Fixed Focus)

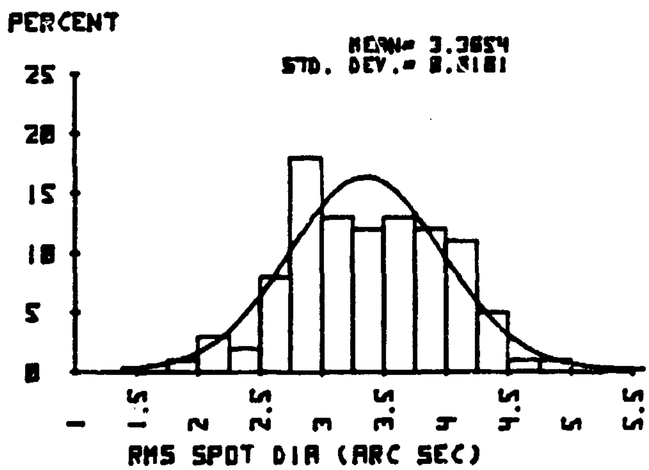

ORIGINAL PAGE IS
OF POOR QUALITY

Fig. 4.5: Probable Performance for the Following Limit Values:
Tilt = 5 μrad
Decenter = 0.005 in.
Despace = 0.001 in.
(On Axis, Fixed Focus)

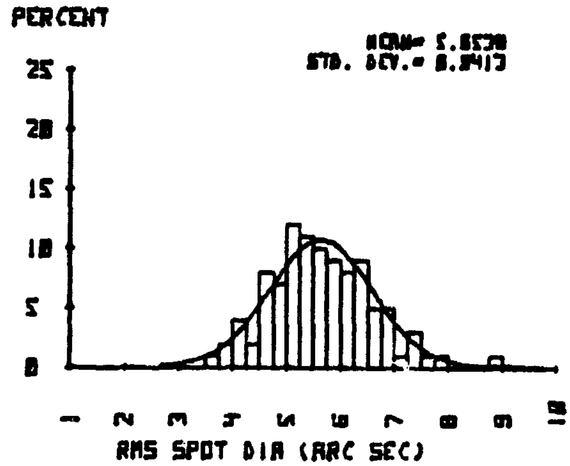

Fig. 4.6: Probable Performance for the Following Limit Values:
Tilt = 10 μrad
Decenter = 0.001 in.
Despace = 0.001 in.
(On Axis, Fixed Focus)

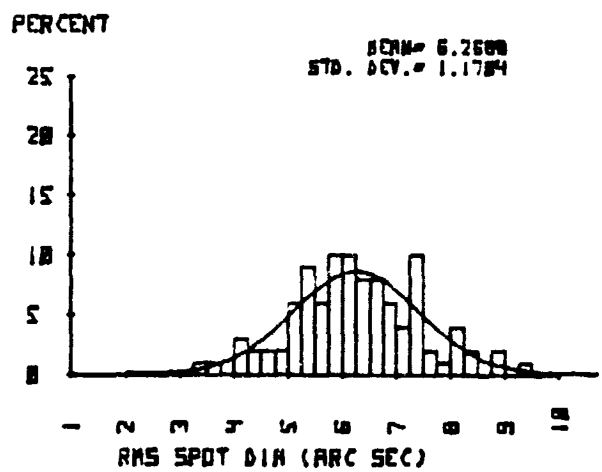

Fig. 4.7: Probable Performance for the Following Limit Values:
Tilt = 2 μrad
Decenter = 0.0002 in.
Despace = 0.0002 in.
(On Axis, Fixed Focus)

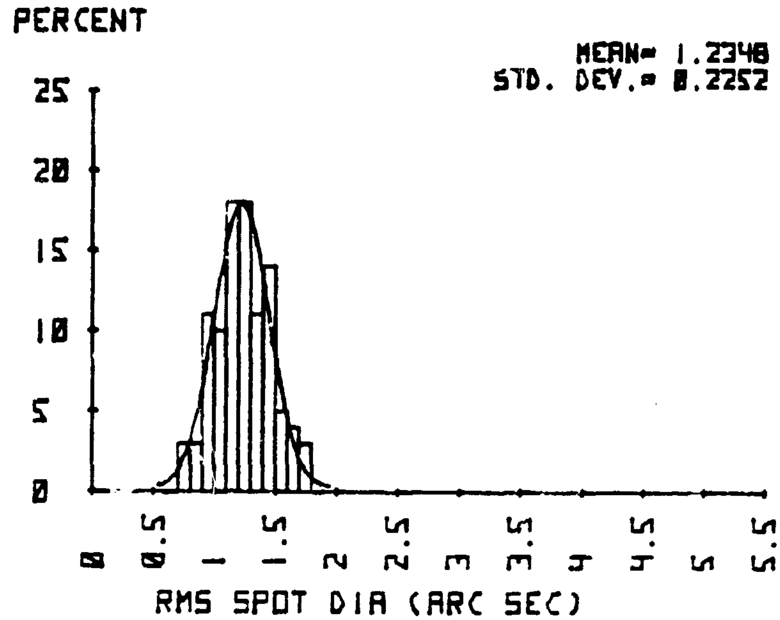

5. COMMENTS ON TESTING THE X-RAY TELESCOPE

To perform a meaningful test of the x-ray telescope, it is desired to have a point source such that the diameter of the on-axis image formed by the telescope does not exceed 1 arcsec. The axial spot diameters as a function of the inverse object distance for two telescope sizes (1.2m and 1.5m) with equal focal lengths of 398.96 in. are plotted in Fig. 5.1.

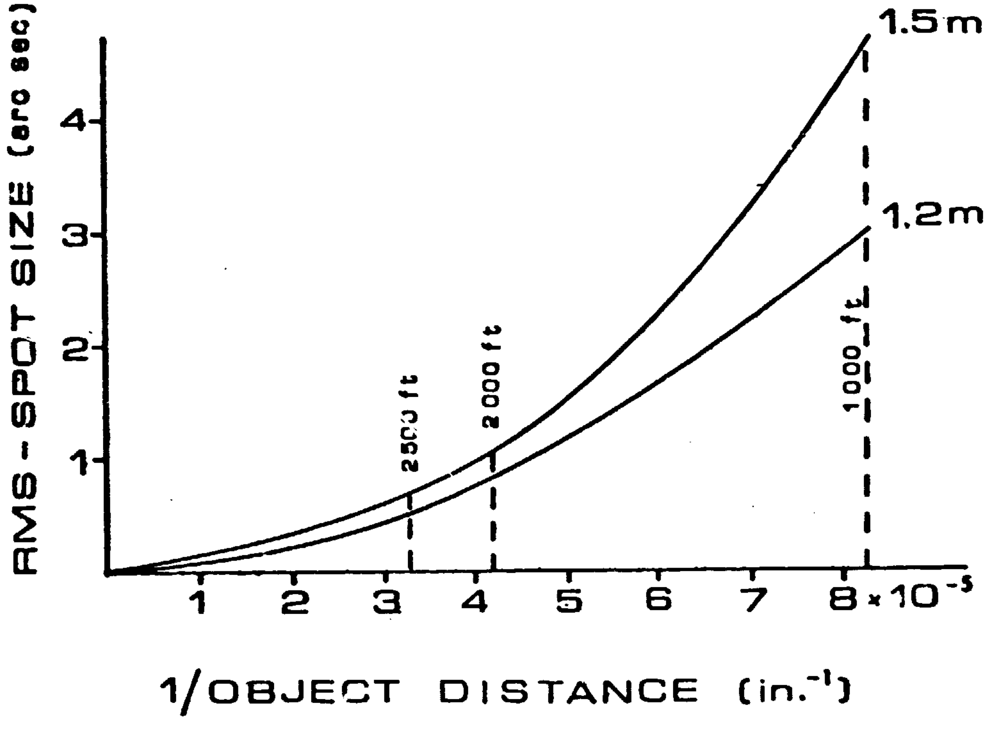

Fig. 5.1: Axial spot size as a function of the object distance for two different telescope sizes.

The associate focal plane shifts, which are the same for both telescope sizes because of the equal focal lengths, are plotted in Fig. 5.2 as a function of the inverse object distance.

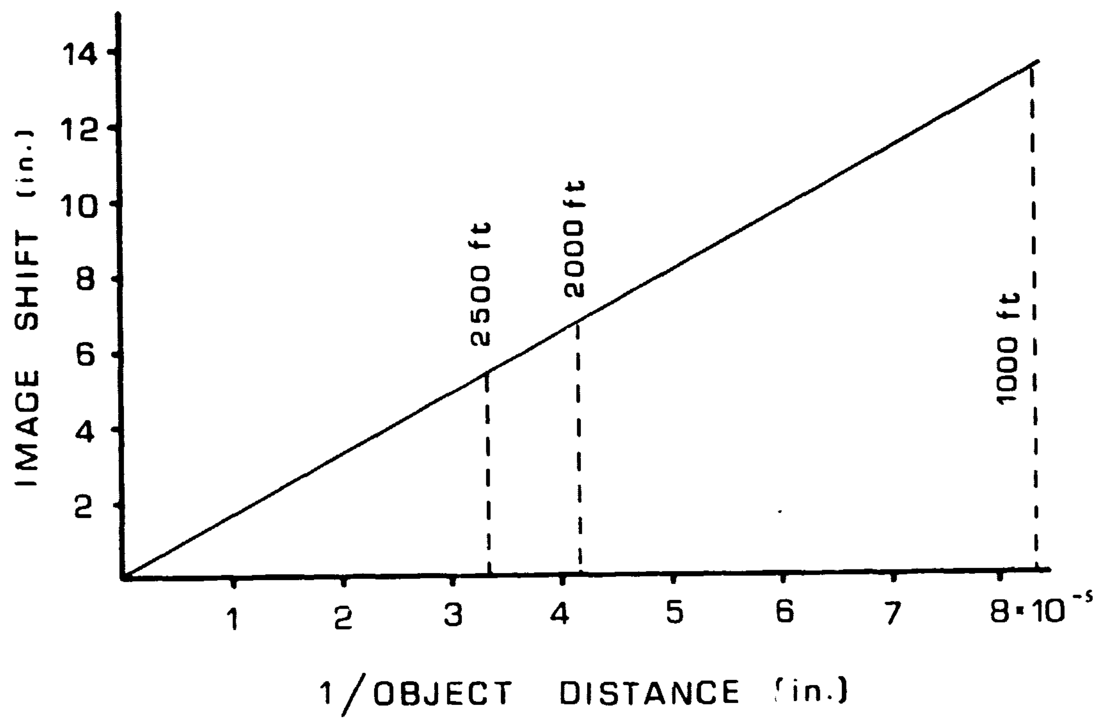

Fig. 5.2: Focal Shift as a Function of the Inverse Object-Distance for Telescopes With a Focal Length of Approximately 400 in.

There are two principle methods to obtain the required spot size. The first and most straightforward method is to select an object distance of at least 2000 or 2500 ft., depending on the telescope size. The second method would be to use a shorter object distance, for instance, the current vacuum tunnel length of 1000 ft., and optically project the source to the desired distance. In the following, methods for an optical extension of the object distance will be discussed.

a) Use of a single hyperbolic element at a distance of 1000 ft. and cover the six subsystems of the telescope assembly subsequently by changing the source distance to the element.

   Comments: The approach has the same inherent problem that the telescope has to begin with, i.e., the single element can only be optimized for one source distance, and thus for only on subsystems of the telescope. Ray trace results show that when this distance changes in order to cover other subsystems, the spot size quickly assumes a diameter of many arcsec.

b) Use a nested system of six single-element hyperbolas to simultaneously cover all six subsystems of the x-ray telescope assembly.

   Comments: The required diameter of the largest element of the test optics is

$$D = Do \left(1 - \frac{1000}{s}\right),$$

where Do is the diameter of the x-ray telescope and s is the desired object distance in ft., assuming the test optics is placed at a distance of 1000 ft. Although this concept is principally workable, there is a problem concerning the required source diameter. For a back focal distance, b, measured from the center of the test array, the source size, Δx, is required to be smaller than $5.10^{-6} \cdot b$ in. in order to obtain a spot size of not larger than 1 arcsec. For example, a back focal distance of 800 in. still requires a source diameter of smaller than 100 μm.

6. APPENDIX

KOGRAZ: A RAY TRACE PROGRAM FOR GRAZING INCIDENCE TELESCOPES

6.1 INTRODUCTION

KOGRAZ is a computer program that analyzes grazing incidence telescopes based on exact ray tracing. The optical system consists of two reflective surfaces the shape of which can be any conic sections of revolution. The program is written in BASIC and performs the following tasks.

1. Computes x, y-coordinates of incident rays on any surface,
2. Determines centroid coordinates of the image spot generated from a point source,
3. Calculates the rms-image diameter of a point source,
4. Determines the Radial Energy Distribution (RED) within an image spot,
5. Determines the image-field curvature,
6. Determines the surface of best focus,
7. Plots spot diagrams.

6.2 THE SURFACE EQUATION

The surface of both elements of two-mirror grazing incidence telescopes are conic sections of revolution (see Fig. 6.1).

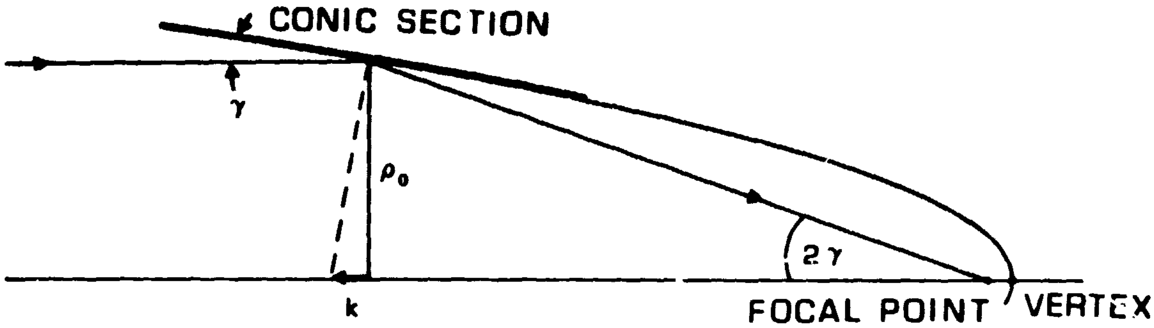

Fig. 6.1: Meridional Section of Grazing Incidence Surface

The surface equation is given by

$$\rho^2 - \rho_0^2 = 2kz - (1 + \delta)z^2, \qquad \rho^2 = x^2 + y^2$$

ρ is the central radius of the element, k is the subnormal at the center and δ is the deformation constant. The type of conic section is determined by the value of δ according to the following list:

$\delta > 0$	Oblate Ellipsoid,
$\delta = 0$	Sphere,
$0 \geq \delta \geq -1$	Prolate Ellipsoid,
$\delta = -1$	Paraboloid,
$\delta < -1$	Hyperboloid.

Since all elements working in grazing incidence have a deformation constant very close to -1, the paraboloid, the prolate ellipsoid and the hyperboloid are the only types of conic sections of revolution to be considered.

It may be interesting to note that the subnormal, k for $\rho_0 = 0$, i.e., in the vertex equation, is identical with the radius of curvature at the vertex.

6.3 THE TWO-MIRROR GRAZING INCIDENCE TELESCOPE

The two-mirror grazing incidence telescope as shown in Fig. 6.2 is completely defined by the following four parameters:

Grazing Angle:	γ (G)
Center Radius of First Mirror:	ρ_{01} (R (1))
Center to Center Separation:	d (D (3))
Half Widths of Entrance Annulus:	$\Delta\rho$ (T)

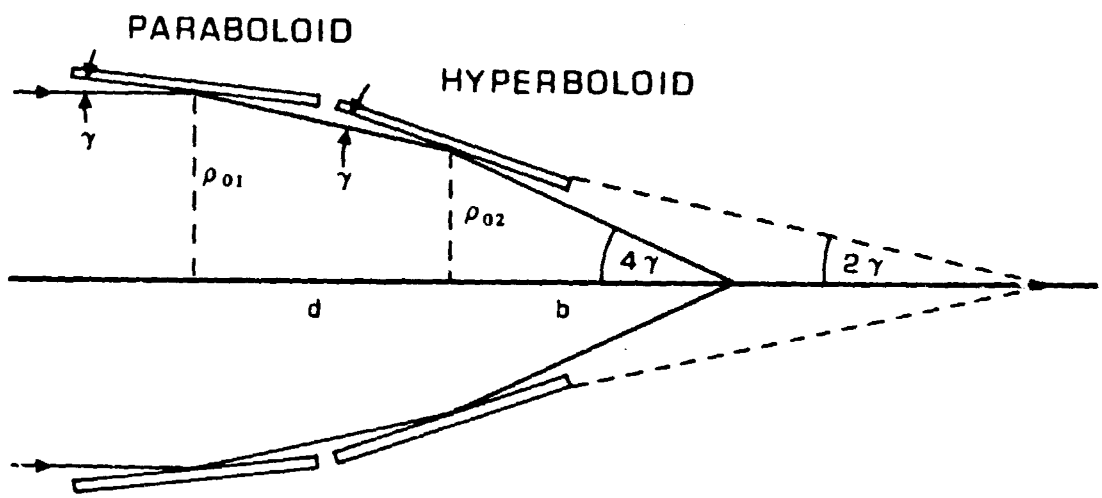

Fig. 6.2: Schematic of Two-Mirror Grazing Incidence Telescope

The bracketed expressions are the corresponding input parameters used in the program. All other quantities can be expressed by using only the first three input parameters. The following is a summary of the most useful system parameters and the relations among them.

Center Radius of Second Mirror:	$\rho_{o2} = \rho_{o1} - d \cdot \tan 2\gamma$
Back Focal Distance (measured from center of second mirror):	$b = \rho_{o2}/\tan 4\gamma$
Center Subnormal of First Surface:	$k_1 = -\rho_{o1} \tan \gamma$
Center Subnormal of Second Surface:	$k_2 = -\rho_{o2} \tan 3\gamma$
Deformation Constant of First Surface:	$\delta_1 = -1$
Deformation Constant of Second Surface:	$\delta_2 = -\left[\dfrac{\sin 2\gamma}{\sin 4\gamma - \sin 2\gamma}\right]^2$
System Focal Length:	$f = 2\rho_{o1}/\sin 8\gamma$
System Focal Ratio:	$F = 1/2 \tan 4\gamma$
Total Length of both Elements:	$L \simeq 2d$

Entrance Aperture: The width of the entrance annulus is calculated by inserting

$$Z = -d/2 \text{ and } Z = + d/2$$

into the equation of the first surface,

$$\rho^2 - \rho_{01}^2 = k_1 Z.$$

a) $\rho = \rho_{01} + \Delta\rho_1$ and $k_1 \simeq \gamma\rho_{01}$.

It then follows: $\rho_{01}^2 + 2\rho_{01}\,\Delta\rho_1 + \Delta\rho_1^2 - \rho_{01}^2 \simeq 2\rho_{01}\,\Delta\rho_1 = 2\gamma\rho_{01}\, d/2$,

or $\Delta\rho_1 \simeq \gamma\, d/2$.

b) $\rho = \rho_{01} - \Delta\rho_2$, and $k_1 \simeq -\gamma\rho_{01}$

It then follows: $\Delta\rho_2 \simeq \gamma\, d/2$.

The half widths of the entrance annulus therefore is to a good approximation,

$$\Delta\rho = \Delta\rho_1 = \Delta\rho_2 = \gamma\, d/2.$$

The collecting area is given by

$$A = \pi(\rho_{01} + \Delta\rho)^2 - \pi(\rho_{01} - \Delta\rho)^2$$

$$= 4\pi\rho_{01}\,\Delta\rho = 2\pi\rho_{01}\gamma d.$$

6.4 INPUT PARAMETERS AND PROCEDURE

The input consists of parameters describing the optical system and the initial parameters defining the set of rays traced through it. The optical system is characterized by its surfaces, their positions and orientations, and the entrance aperture.

A summary of all pertinent input parameters is listed below.

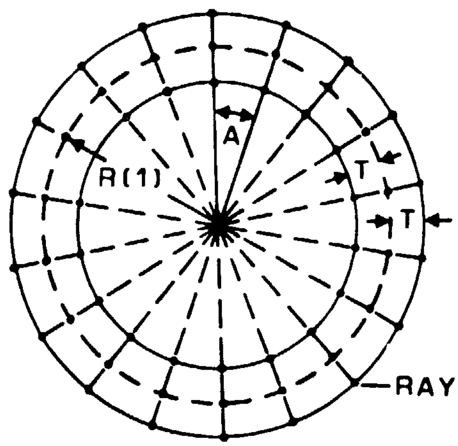

Fig. 6.3: Ray Coordinates in Entrance Aperture

Fig. 6.3 explains the ray distribution in the entrance annulus. T is the radial ray separation and A is the angular tangential ray separation. A is generally calculated so that the linear tangential ray separation equals T.

TABLE 6.1: Input Parameters

Name	Description	Line-No.
J	Total number of surfaces, (incl. dummy surfaces)	10
G	Grazing angle at center of each surface (rad)	40
GO	Off-axis angle in XZ-plane, (rad)	50
HO	Off-azis angle in YZ-plane, (rad)	55
SO	Divider of T	60
T	Half width of entrance annulus	70
A	Ray input parameter, (rad), (See Fig. 3)	80
MO	Inverse object distance (MO = 0 for telescope)	90
P1	Starting point for RED in percent	95
PO	Increment of RED in percent	96
R(1)	Center Radius of first surface	170
D(1)	Distance from entrance aperture to center of first surface	180
D(3)	Mirror center to center separation	190
F	Unit selector for image size { F = 1 [linear units]; F = Focal length [rad]; F = JO·Focal length/3600 [arcsec] }	450
S(3)	Tilt of secondary about X-axis, (rad)	} 460
T(3)	Tilt of secondary about Y-axis, (rad)	} -490
G(3)	Decenter of secondary in x-direction	}
H(3)	Decenter of secondary in Y-direction	}
C(3)	Despace primary - secondary	}
C(5)	Defocus	}

Finally there are the subroutines which are those parts of the program that perform the tasks listed in the introduction. After loading the program, all subroutines are bypassed using a "GOTO" statement. A temporary elimination of this statement makes the corresponding subroutine available. The following listing summarizes all possible print-out options:

TABLE 6.2: Print Out Options

Parameter listing	300 GOTO 450
Ray coordinates in entrance plane and on J-th surface	1380 GOTO 1440
Best-Focus computation	1580 GOTO 1740
Centroid coordinates Field-curvature, RMS-Spotsize	1760 GOTO 1910
Radial Energy Distribution	1920 GOTO 2240
Percent of rays through specified exit aperture	2270 GOTO 2300

ORIGINAL PAGE IS
OF POOR QUALITY

6.5 PROGRAM LISTING

```
1 REM ********************KOGRAZ********************
10 J=5
20 J0=ATN(1)/45
30 F=J0*399/3600
40 G=0.015
50 G0=0
55 H0=0
60 S0=2
70 T=0.245
80 A=18*J0
90 M0=0
95 P1=60
96 P0=10
100 DIM U(500),V(500),X(500),Y(500)
110 DIM A(500),B(500),R(500),Z(500)
120 FOR N=1 TO J
130 R(N)=0,L(N)=0,D(N)=0,G(N)=0,H(N)=0,S(N)=0,T(N)=0,C(N)=0
140 K(N)=1
150 E(N)=-1
160 NEXT N
170 R(1)=23.88
180 D(1)=16.5
190 D(3)=35.076158
200 K(1)=-1,K(3)=-1
210 A1=2*G
220 A2=4*G
230 R(3)=R(1)-D(3)*TAN(A1)
240 D(5)=R(3)/TAN(A2)
250 E(3)=-(SIN(A2-A1)/(SIN(A2)-SIN(A1)))^2
260 L(1)=-R(1)*TAN(A1/2)
270 L(3)=-R(3)*TAN(A1/2+A2/2)
275 F=2*R(1)/SIN(8*G)
280 IF G0+H0=0 THEN 290
284 PRINT
285 PRINT "FIELD ANG:G0="G0,"H0="H0
286 PRINT
290 REM**********DESIGN PARAMETERS**********
300 GOTO 450
330 PRINT
340 PRINT "GRAZ ANG  :";G
350 PRINT
360 PRINT "RAD OF EL :";R(1),R(3)
390 PRINT
400 PRINT "SEPARATION:";D(1),D(3),D(5)
410 PRINT
420 PRINT "K-CONSTANT:";L(1),L(3)
430 PRINT
440 PRINT "D-CONSTANT:";E(1),E(3)
441 PRINT
445 PRINT "FOCAL LENGTH:"F, "       T:"T
450 F=F
```

```
500 W3=0,M=0,N=0
510 FOR RO=R(1)-T TO R(1)+T STEP T
520 FOR B=A TO 360*JO STEP A
530 XO=RO*COS(B)
540 YO=RO*SIN(B)
550 X=XO
560 Y=YO
570 Z=0
580 K5=TAN(GO)-MO*X
590 L5=TAN(HO)-MO*Y
600 CO=1/SQR(1+K5^2+L5^2)
610 AO=K5*CO
620 BO=L5*CO
630 FOR I=1 TO J
640 D1=G(I)
650 D2=H(I)
660 D3=D(I)+C(I)
670 W1=S(I)
680 W2=T(I)
690 R=L(I)
700 D=E(I)
710 K=K(I)
720 IF W1*W1+W2*W2+W3*W3=0 THEN 830
730 A1=COS(W2)*COS(W3)
740 B1=COS(W1)*SIN(W3)+SIN(W1)*SIN(W2)*COS(W3)
750 C1=SIN(W1)*SIN(W3)-COS(W1)*SIN(W2)*COS(W3)
760 A2=-COS(W2)*SIN(W3)
770 B2=COS(W1)*COS(W3)-SIN(W1)*SIN(W2)*SIN(W3)
780 C2=SIN(W1)*COS(W3)+COS(W1)*SIN(W2)*SIN(W3)
790 A3=SIN(W2)
800 B3=-SIN(W1)*COS(W2)
810 C3=COS(W1)*COS(W2)
820 GOTO 850
830 A1=1,B2=1,C3=1
840 A2=0,A3=0,B1=0,B3=0,C1=0,C2=0
850 X1=A1*(X-D1)+B1*(Y-D2)+C1*(Z-D3)
860 Y1=A2*(X-D1)+B2*(Y-D2)+C2*(Z-D3)
870 Z1=A3*(X-D1)+B3*(Y-D2)+C3*(Z-D3)
880 A4=AO*A1+BO*B1+CO*C1
890 B4=AO*A2+BO*B2+CO*C2
900 C4=AO*A3+BO*B3+CO*C3
910 IF R=0 THEN 1020
930 S1=D+1/C4^2
940 S2=R-A4*(X1-A4*Z1/C4)/C4-B4*(Y1-B4*Z1/C4)/C4
950 S3=(X1-A4*Z1/C4)^2+(Y1-B4*Z1/C4)^2-R(I)^2
1000 Z=S3/(S2*(1+SQR(1-S1*S3/S2^2)))
1010 GOTO 1030
1020 Z=0
1030 X=A4*(Z-Z1)/C4+X1
1040 Y=B4*(Z-Z1)/C4+Y1
1050 IF R=0 THEN 1110
1060 P=R-(1+D)*Z
1070 Z2=X/P
1090 Z3=Y/P
1100 GOTO 1125
1110 Z2=0
1120 Z3=0
1125 Z4=SQR(Z2*Z2+Z3*Z3+1)
```

```
1130 A5=Z2/Z4
1140 B5=Z3/Z4
1150 C5=-1/Z4
1160 V=A4*A5+B4*B5+C4*C5
1200 U=V*(1-K)/K
1220 A0=A4/K-U*A5
1230 B0=B4/K-U*B5
1240 C0=C4/K-U*C5
1250 IF I<>1 THEN 1270
1260 M=M+1
1270 NEXT I
1280 N=N+1
1290 U(N)=X0
1300 V(N)=Y0
1310 X(N)=X
1320 Y(N)=Y
1330 A(N)=A0/C0
1340 B(N)=B0/C0
1350 NEXT B
1360 NEXT R0
1370 REM **********RAY COORDINATES**********
1380 GOTO 1440
1390 PRINT "  X0              Y0              X              Y"
1400 PRINT
1410 FOR J=1 TO N
1420 PRINT U(J),V(J),X(J),Y(J)
1430 NEXT J
1440 PRINT
1450 X9=0,Y9=0,A9=0,B9=0
1460 FOR J=1 TO N
1470 X9=X9+X(J)
1480 Y9=Y9+Y(J)
1490 A9=A9+A(J)
1500 B9=B9+B(J)
1510 NEXT J
1520 X9=X9/N
1530 Y9=Y9/N
1540 A9=A9/N
1550 B9=B9/N
1560 Z9=0
1570 REM **********BEST FOCUS**********
1580 GOTO 1740
1590 Z7=0,Z8=0
1600 FOR J=1 TO N
1610 Z7=Z7+(X(J)-X9)*(A(J)-A9)+(Y(J)-Y9)*(B(J)-B9)
1620 Z8=Z8+(A(J)-A9)^2+(B(J)-B9)^2
1630 NEXT J
1640 Z9=-Z7/Z8
1650 X9=0,Y9=0
1660 FOR J=1 TO N
1670 X(J)=X(J)+A(J)*Z9
1680 Y(J)=Y(J)+B(J)*Z9
1690 X9=X9+X(J)
1700 Y9=Y9+Y(J)
1710 NEXTJ
1720 X9=X9/N
1730 Y9=Y9/N
1740 REM
```

```
1750 REM **********CENTROID FIELD-CURV RMS-SPOT SIZE**********
1760 GOTO 1910
1770 R8=0
1780 FOR J=1 TO N
1790 R8=R8+(X(J)-X9)^2+(Y(J)-Y9)^2
1800 NEXT J
1810 R9=SQR(R8/N)
1820 PRINT "CENTROID X=";X9
1830 PRINT "CENTROID Y=";Y9
1840 PRINT "    DELTA Z=";Z9
1850 PRINT
1860 IF G0^2+H0^2=0 THEN 1880
1870 PRINT "FIELD-CURV=";2*Z9/(X9^2+Y9^2)
1880 PRINT
1890 R9=R9/F
1900 PRINT "RMS-DIA :";2*R9
1910 PRINT
1920 GOTO 2240
1925 FOR J=1 TO N
1930 Z(J)=SQR((X(J)-X9)^2+(Y(J)-Y9)^2)
1940 NEXT J
1950 FOR K=1 TO N
1960 D=Z(1)
1970 M1=0
1980 FOR J=2 TO N-K+1
1990 IF Z(J)>D THEN 2030
2000 Z(J-1)=D
2010 D=Z(J)
2020 GOTO 2060
2030 E=Z(J)
2040 Z(J)=Z(J-1)
2050 Z(J-1)=E
2060 NEXT J
2070 R(K)=D
2080 NEXT K
2090 REM **********RADIAL ENERGY DISTRIBUTION**********
2110 PRINT "RADIAL ENERGY DISTRIBUTION:"
2120 PRINT
2130 PRINT " %                        DIA"
2140 PRINT
2150 I1=0
2160 FOR I0=P1 TO 100 STEP P0
2170 FOR I=I1+1 TO N
2180 IF I*100/N<I0 THEN 2220
2190 PRINT I0,2*R(I)/F
2200 I1=I
2210 GOTO 2230
2220 NEXT I
2230 NEXT I0
2240 PRINT
2250 PRINT "NO. OF RAYS:";N
2260 REM **********PERCENT OF RAYS THROUGH EXIT APERTURE**********
2270 GOTO 2300
2280 PRINT
2290 PRINT N*100/M;"% THROUGH EXIT APERTURE"
2300 PRINT
9999 END
```